JACS
JOURNAL OF THE AMERICAN CHEMICAL SOCIETY
Article
Cite This: J. Am. Chem. Soc. 2018, 140, 16580−16588
pubs.acs.org/JACS

BCC-Phased PdCu Alloy as a Highly Active Electrocatalyst for Hydrogen Oxidation in Alkaline Electrolytes

Yang Qiu,[†,‡] Le Xin,[†,‡] Yawei Li,[§,‡] Ian T. McCrum,[§] Fangmin Guo,[∥] Tao Ma,[⊥] Yang Ren,[∥] Qi Liu,[∥] Lin Zhou,[⊥] Shuang Gu,[#] Michael J. Janik,[§] and Wenzhen Li*[,†,⊥]

[†]Department of Chemical and Biological Engineering, Iowa State University, 618 Bissell Road, Ames, Iowa 50011, United Sates
[§]Department of Chemical Engineering, Pennsylvania State University, 51 Greenberg Building, University Park, Pennsylvania 16802, United States
[∥]Advanced Photon Source, Argonne National Laboratory, 9700 South Cass Avenue, Argonne, Illinois 60439, United States
[⊥]Ames Laboratory, U.S. Department of Energy, 311 Iowa State University, Ames, Iowa 50011, United States
[#]Department of Mechanical Engineering, Wichita State University, 1845 Fairmount St. Wichita, Kansas 67260, United States

Supporting Information

ABSTRACT: Anion-exchange membrane fuel cells hold promise to greatly reduce cost by employing nonprecious metal cathode catalysts. More efficient anode catalysts are needed, however, to improve the sluggish hydrogen oxidation reaction in alkaline electrolytes. We report that BCC-phased PdCu alloy nanoparticles, synthesized via a wet-chemistry method with a critical thermal treatment, exhibit up to 20-fold HOR improvement in both mass and specific activities, compared with the FCC-phased PdCu counterparts. HOR activity of the BCC-phased PdCu is 4 times or 2 times that of Pd/C or Pt/C, respectively, in the same alkaline electrolyte. In situ HE-XRD measurements reveal that the transformation of PdCu crystalline structure favors, at low annealing temperature (<300 °C), the formation of FCC structure. At higher annealing temperatures (300−500 °C), a BCC structure dominates the PdCu NPs. Density functional theory (DFT) computations unravel a similar H binding strength and a much stronger OH binding of the PdCu BCC surface (cf. FCC surface), both of which are simultaneously close to those of Pt surfaces. The synergistic optimization of both H and OH binding strengths is responsible for the enhancement of HOR activity on BCC-phased PdCu, which could serve as an efficient anode catalyst for anion-exchange membrane fuel cells. This work might open a new route to develop efficient HOR catalysts from the perspective of crystalline structure transformation.

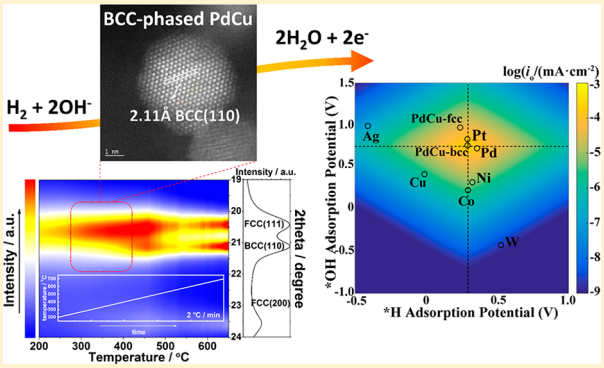

INTRODUCTION

Offering alkaline environments, anion-exchange membrane fuel cells (AEMFCs) allow long-time catalytic operation of inexpensive nonprecious metals and their alloys, which can significantly reduce the cost of fuel cell systems.[1,2] This cost reduction is particularly encouraged by the oxygen reduction reaction (ORR) at the cathode, because non-noble metal catalysts have shown activity comparable to that of the state-of-the-art ORR catalyst Pt in AEMFCs.[3−5] However, the activities of the anode reaction, hydrogen oxidation reaction (HOR), are at least 2 orders of magnitude lower on Pt-group metals in alkaline electrolytes (e.g., the exchange current density, i_0: ∼ 1 mA cm^{-2}_{Pt} at 40 °C on Pt/C) than in acidic electrolyte (e.g., i_0: ∼ 120 mA cm^{-2}_{Pt} at 40 °C on Pt/C), consequently requiring much higher Pt-group metal loading for AEMFCs in comparison to proton exchange membrane fuel cells (PEMFCs).[6−8] Therefore, motivated by achieving a comparable HOR activity in AEMFCs to compete with PEMFCs, the mechanism of HOR on transition metals has been extensively studied.[1,2]

Trasatti and Nørskov groups proposed an empirical correlation between the exchange current densities of HOR and the hydrogen adsorption energies (derived from the differential Gibbs free energy of hydrogen adsorption, ΔG_{H^*}) on different metals, and a volcano relationship was constructed.[9−11] An active HOR catalyst should bind hydrogen neither too strongly nor too weakly. With an "optimal" hydrogen binding strength, Pt-group metals (e.g., Pt, Pd, Ir, Rh, etc.) are highly active catalysts toward HOR. However, this simplistic view does not help to differentiate the HOR activity between acidic and alkaline electrolytes. There are conflicting interpretations of the inferior HOR performance in alkaline environments, despite intense recent research efforts. Sheng et al. correlated the experimentally measured HOR exchange

Received: August 5, 2018
Published: November 5, 2018

DOI: 10.1021/jacs.8b08356
J. Am. Chem. Soc. 2018, 140, 16580−16588

current densities of a series of monometals in alkaline electrolyte with their calculated hydrogen binding energy (HBE) and found that most monometallic catalysts possess stronger hydrogen binding in base than in acid.[12] Therefore, they suggested that the HBE could be a major descriptor in alkaline electrolyte and that the slower kinetics can be mainly ascribed to a generally strengthened H adsorption in alkaline environments.[13,14] On the other hand, Strmcnik et al. argued that the oxophilic nature of catalyst surfaces (OH binding energy) also played a significant role in alkaline HOR, as evidenced by Ir and PtRu catalysts that outperformed Pt toward HOR in alkaline electrolyte.[15] The oxophilic effect of Ru and Ir was demonstrated by low OH adsorption potential, enabling the oxidative removal of adsorbed hydrogen. The decoupling of HBE from HOR rate on Pt−Ru/C and Ru/C systems is also validated by electrochemical measurements and kinetic studies which provide evidence of surface hydroxyl groups on Ru surface sites participating in a bifunctional mechanism.[16] The underpotential-deposited hydrogen desorption peak potential has been suggested to directly correlate with HBE, and the CO-stripping has been suggested to directly relate to the OH binding energy.[13,14,17] Nevertheless, no DFT work or fundamental surface studies have suggested that the strength of H binding to metals changes with pH, and to the contrary, the work of the Janik group has suggested that changing pH (and the accompanying change to include cations in the near surface region) contributes very little effect on H-metal interactions but more effect on OH surface stability.[18] Their calculations are further corroborated by a recent experimental study suggesting that the "hydrogen region" on a Pt stepped electrode is actually a "hydrogen−hydroxyl−cation" region and that the observed "hydrogen peak" shift with pH is caused by cation−hydroxyl coadsorption.[19] Chuang et al. also found that the specific chemisorption of organic cations can drive the hydroxide coadsorption on the Pt surface, leading to decreased HOR activity.[20] These observations collectively lead to a major discrepancy in approaches to rational alkaline HOR catalyst design—whether *H stability alone is sufficient to predict activity or does *OH adsorption/oxophilicity act as a second independent descriptor.

We hypothesize that development of the highly active HOR catalysts in alkaline media requires modification and optimization of both H and OH adsorption. Guided by the volcano relationship between HOR activity and HBE, Pt-group metal based binary catalysts are investigated with a second metal introduced to reduce the strength of hydrogen adsorption. Wong et al. rationally designed Pt/M (M = Ru, Co, Fe, Cu, and Au) as HOR catalysts and reported that hydrogen adsorption on PtRu, PtFe, PtCo, and PtCu was weakened with the second metal incorporation, whereas PtAu was expected to be strenghened.[21] In addition, Greeley et al. demonstrated that a transition metal substrate could significantly change the hydrogen adsorption strength to a Pd surface, and Pd/PtRu shows an optimal hydrogen adsorption ability thereby exhibiting 1 order of magnitude higher HOR exchange current density than other investigated Pd/M catalysts (M = Re, Ru, Ir, Rh, Pt, Au).[22]

However, little research effort has been made to explore the crystalline structure of metal and metal alloy catalysts for HOR in alkaline electrolyte. From a structural perspective, a crystalline structure with a different lattice constant can significantly influence hydrogen and/or hydroxyl adsorption strengths, thus altering their overall activity for a specific reaction (e.g., enhanced activity of ORR and ethanol oxidation reaction on BCC-structured PdCuCo and PdCuNi materials).[23]

Herein we prepared PdCu alloy nanoparticles (NPs) and characterized the HOR activity in 0.1 M KOH solution. The HOR activity exhibited a strong dependence on the crystalline structure governed by the annealing temperature. In particular, PdCu alloy NPs annealed at 500 °C exhibit very high mass and specific activities, outperforming all as-synthesized Pd, PdCu, and even commercial Pt catalysts. The transformation of PdCu crystalline structure from face-centered cubic (FCC) to body-centered cubic (BCC) was observed as the thermal annealing temperature increased from 200 °C to 600 °C, and the correlation between the HOR performances and the crystalline structures as well as their strength with H and OH was further investigated by DFT computations. Specifically, H adsorption potential on a PdCu BCC surface are closer to those on a PdCu FCC surface, while the much stronger OH adsorption on PdCu BCC surface causes the BCC phase to exhibit an HOR catalytic performance much higher than that of the FCC.

RESULTS AND DISCUSSION

Catalysts Synthesis and Physical Characterizations. The PdCu NPs were synthesized following a one-step wet-chemistry method via a fast reduction of equal molar amounts of Pd(II) and Cu(II) precursors.[24] To mitigate the particle agglomeration, carbon support (carbon black) was introduced at the beginning of the synthesis process, and PdCu NPs were deposited on carbon black, yielding PdCu/C-raw. As shown in Figure 1a, PdCu NPs were found to be evenly dispersed on the surface of carbon black, and the particle size was well controlled at ca. 4.7 nm with a narrow size distribution (3.5 to 6.5 nm). Due to such a small particle size, only two broad diffraction peaks at 41.7° and 48.4° were distinguished from the PdCu/C-raw XRD pattern, which can be indexed to (111) and (200) reflections of face-centered cubic (FCC) PdCu (ICDD 00-048-1551) (Figure 1b). The absence of monometallic Pd and Cu diffraction peaks indicates that the PdCu NPs were well-alloyed with the FCC crystalline structure.

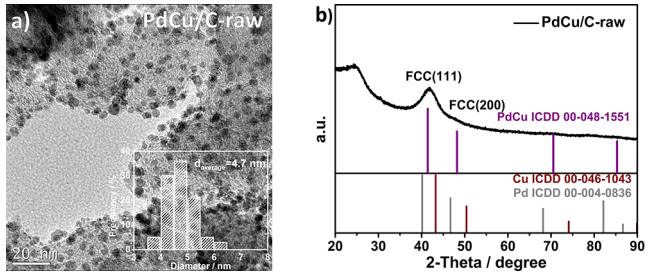

Figure 1. (a) TEM image and (b) XRD pattern of PdCu/C-raw sample. The inset of panel a is particle diameter histograms of PdCu/C-raw sample.

Electrochemical Characterizations. The HOR activity of as-synthesized PdCu/C-raw, Pd/C, Cu/C, and commercial Pt/C was evaluated by using rotating disk electrode (RDE) voltammetry in H_2-saturated 0.1 M KOH electrolyte at room temperature and ambient pressure. HOR/HER polarization curves were compensated by the electrolyte resistance measured before testing, and the kinetic current density, J_k, was calculated based on the Koutecky−Levich equation (see Supporting Information).[25] Although the kinetics of HOR in

DOI: 10.1021/jacs.8b08356
J. Am. Chem. Soc. 2018, 140, 16580−16588

acid electrolyte was too fast to be determined by using regular RDE technique, the RDE measurement can well describe the kinetics of HOR in base.[26] As shown in Figure 2a and 2b, Pd/C exhibits a moderate HOR activity among all investigated monometallic catalysts, which follows the order of Pt/C > Pd/C > Cu/C (nearly inactive toward HOR). The half-wave potential of Pd/C was measured to be 0.069 V at 1600 rpm, and this is very close to the result of 0.070 V reported by Zheng et al.[25] According to the hypothesis that incorporated Cu could help optimize H and OH adsorption strengths relative to pure Pd, PdCu/C-raw was expected to show an HOR activity higher than that of Pd/C in alkaline solution. Unexpectedly, a fairly inferior HOR activity with a much larger half-wave potential of 0.204 V was obtained over PdCu/C-raw. We further applied thermal annealing to obtain PdCu/C-*T* samples (*T* = 200 °C, 300 °C, 400 °C, 500 °C, and 600 °C). The HOR activity of PdCu/C samples was much improved after the thermal annealing at 300 °C to 500 °C. Among all thermally annealed PdCu/C samples, PdCu/C-500 °C exhibits the highest HOR activity with a much smaller half-wave potential of 0.028 V as compared to 0.069 V of Pd/C and 0.047 V of Pt/C. With further increased annealing temperature, the HOR activity of PdCu/C-600 °C ($E_{1/2}$ = 0.184 V) was largely reduced, approaching that of PdCu/C-raw ($E_{1/2}$ = 0.204 V) and PdCu/C-200 °C ($E_{1/2}$ = 0.145 V).

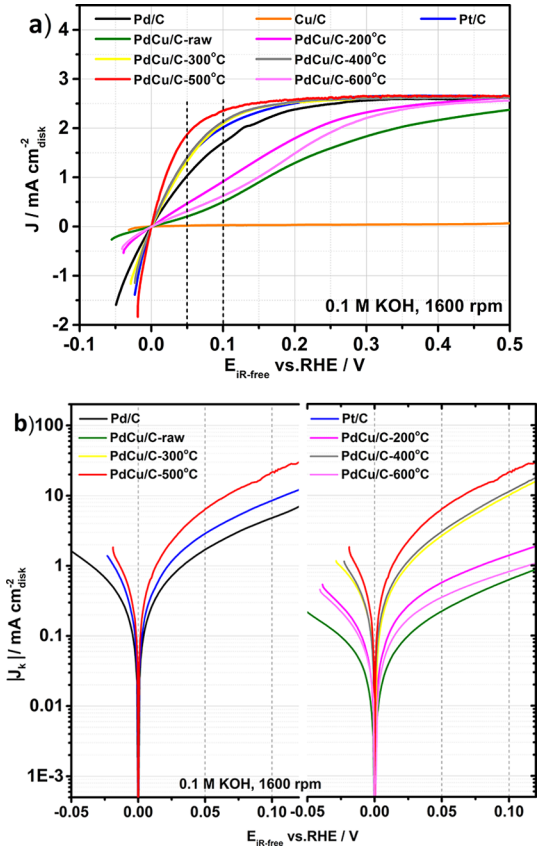

Figure 2. (a) HOR/HER polarization curves (forward scan) and (b) representative Tafel plots of Pt/C, Pd/C, Cu/C, and PdCu/C materials measured at a scanning rate of 1 mV/s in H_2-saturated 0.1 M KOH electrolyte with *iR* correction under 1600 rpm.

To obtain the surface-specified activity, we measured the electrochemical surface area (ECSA). Integration of the PdO reduction peak is the most commonly used method to determine the ECSA of Pd-based catalysts.[27,28] However, the Cu(I) reduction peak was found to overlap with the PdO reduction peak in the potential range of 0.420 to 0.720 V (Figure S1), thus causing an ECSA overestimation of Pd for as-synthesized PdCu/C catalysts.[29] Therefore, a CO-stripping method was employed to measure the ECSA of active Pd (or Pt) for all investigated catalysts in this work, and all measured ECSA results are summarized in Table S1 (for details of CO-stripping measurement, see Supporting Information).[28,30] The specific activity (SA) was then normalized by measured ECSA of active Pd (or Pt).

As shown in Figure 3, the mass activity (MA) and the specific activity (SA) were determined at 100 mV overpotential (for details of MA and SA calculation, see Supporting Information). Among all studied catalysts, PdCu/C-500 °C exhibits the highest MA of 1.727 mA μg_{Pd}^{-1} and SA of 2.922 mA cm^{-2}_{Pd} at 100 mV overpotential, which is about 2 times as much as those of Pt/C (MA of 0.680 mA μg_{Pt}^{-1}, SA of 1.525 mA cm^{-2}_{Pt}) and 4 times as much as those of Pd/C (MA of 0.385 mA μg_{Pd}^{-1}, SA of 0.623 mA cm^{-2}_{Pd}), respectively, and much higher than those of other PdCu/C samples. Similar results were also obtained at 50 mV overpotential, indicating the outstanding HOR activity of PdCu/C-500 °C (Figure S2). These results were further compared with other HOR catalysts reported in previous work (Table S2), and the activity of the as-synthesized PdCu/C-500 °C stays on the top among reported noble metal-based HOR catalysts. In addition, a robust stability of as-synthesized PdCu/C-500 °C was obtained by a chronoamperometry test at 100 mV overpotental

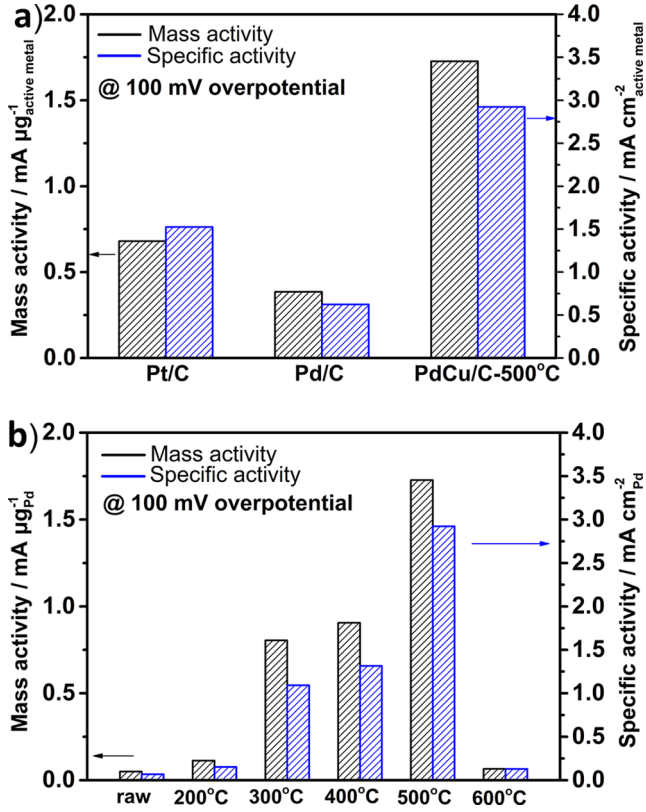

Figure 3. Comparison of HOR mass and specific activity (MA and SA) of Pt/C, Pd/C, and PdCu/C at 100 mV overpotential in H_2-saturated 0.1 M KOH electrolyte.

DOI: 10.1021/jacs.8b08356
J. Am. Chem. Soc. 2018, 140, 16580−16588

for 12 h in 0.1 M KOH solution (Figure S3). By taking the low catalyst cost into consideration, as-synthesized PdCu/C-500 °C catalysts would be quite promising to serve as the HOR catalysts in AEMFCs.

Structure Analysis for Elucidating Enhanced HOR Activity. Prior to the PdCu NP structure analysis, it is important to note that most organic complexes (surfactants) involved in the synthesis process were effectively removed by thermal annealing, and the obtained cyclic voltammogram of thermal-annealed PdCu/C samples should not be influenced by surfactant.[31] As shown in Figure S4, two weight loss steps were observed from TGA curves, including the evaporation and desorption of absorbed water from the catalyst surface at 70 °C to 170 °C and surfactant desorption and gradual decomposition at 170 °C to 600 °C.[32] During thermal annealing, PdCu/C-*T* (*T* = 200 °C to 600 °C) catalysts exhibit very close weight loss of <3 wt % between 170 °C to 600 °C which is much smaller than ∼10 wt % weight loss of PdCu/C-raw sample, indicating that the thermal annealing process can effectively remove the organic surfactants and water residue existed in PdCu catalysts, and the low HOR activity of PdCu/C-200 °C and PdCu/C-600 °C cannot be attributed to surfactant residue.

To understand the reason for the improved HOR activity on PdCu/C-500 °C after thermal annealing, the PdCu NP morphology and composition were first analyzed. The transmission electron microscopy (TEM) images reveal a good dispersion of PdCu NPs on carbon support over all PdCu/C-*T* (*T* = 200 °C to 600 °C) catalysts. Very slight particle agglomeration was observed with increasing annealing temperature, as the PdCu particles grew from 4.7 nm (PdCu-200 °C) to 7.0 nm (PdCu-500 °C) as shown in Figure 4a–d.

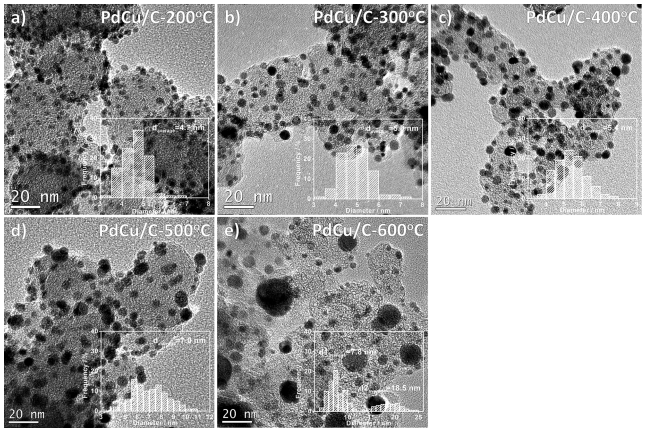

Figure 4. TEM images and particle diameter histograms (inset) of PdCu/C-*T* (*T* = 200 °C to 600 °C).

When the temperature was further increased to 600 °C, agglomerated PdCu particles with 18.5 nm diameter were observed (Figure 4e). Figure 5 shows the high-angle-annular-dark-field STEM (HAADF-STEM) images and corresponding energy-dispersive X-ray spectroscopy (EDS) element mapping and line scan images of representative PdCu NPs treated at 200 °C and 500 °C. It is obvious that Pd and Cu species were uniformly distributed throughout PdCu NPs, indicating well alloyed PdCu NPs rather than a core–shell structure. A Pd-rich surface was observed on both PdCu/C-200 °C and PdCu/C-500 °C samples from EDS element mapping and line scan images, which could be caused by a Pd atomic concentration

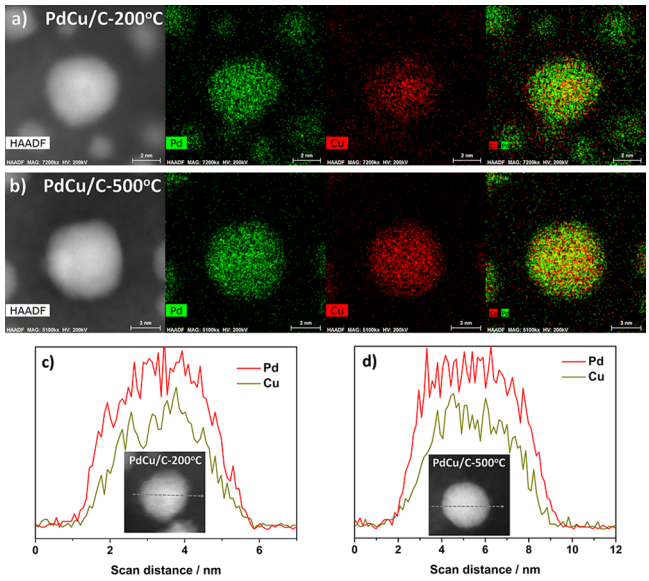

Figure 5. High-resolution HAADF STEM images with EDS element mapping and line scanning results: (a, c) PdCu/C-200 °C, and (b, d) PdCu/C-500 °C.

slightly higher than that of Cu in PdCu NPs. As confirmed by inductively coupled plasma optical emission spectrometry (ICP-OES), the PdCu composition (bulk composition) varies slightly from 56.5 at. %/43.5 at. % (Pd/Cu) of PdCu/C-200 °C to 55.8 at. %/44.2 at. % (Pd/Cu) of PdCu/C-600 °C (Table S3) and is very close to the setting ratio of 50 at. %/50 at. %. Less than 1% Pd/Cu composition change due to annealing could make very little contribution to HOR activity enhancement of PdCu/C-500 °C via thermal annealing.

The PdCu NPs were further studied by XPS. As compared with Pd/C, Pd $3d_{5/2}$ and Pd $3d_{3/2}$ peaks of all PdCu/C samples shift to lower binding energy of 335.3 eV (Pd $3d_{5/2}$) and 340.6 eV (Pd $3d_{3/2}$) (Figure S5), which can be ascribed to an electron negativity of Cu smaller than that of Pd.[33] However, no apparent binding energy shift of Pd $3d_{5/2}$ or Pd $3d_{3/2}$ peaks was observed among all PdCu/C catalysts, suggesting that the lack of Pd–Cu phase segregation and surface composition change caused electronic structure variation. These observations further indicate that thermal annealing has very little effect on PdCu electronic structure and composition change, and the alloy state of PdCu NPs can be well maintained during thermal annealing, without signs of Pd–Cu phase segregation or core–shell structure formation. Therefore, the promoted HOR activity of PdCu/C-300 °C, PdCu/C-400 °C, and PdCu/C-500 °C unlikely comes from structure or composition variation after heat treatment.

The size effect was also considered in this work. Owing to different binding strengths of the specific species on surface sites and edge sites, the particles with different sizes could exhibit specific activities. When the particle size is smaller than the critical size (normally <4.0 nm), the particle size has substantial effects on area-specific catalytic activities.[34−36] In this work, the particle size of all PdCu/C catalysts (4.7 to 18.5 nm) is bigger than the critical size, suggesting that the improved HOR activity observed in this work cannot be attributed to difference in particle size. As the thermal annealing temperature was raised from 200 °C to 300 °C, the average particle size increased slightly from 4.7 to 5.0 nm; however, the SA drastically increased to 7.2 times at 100 mV

DOI: 10.1021/jacs.8b08356
J. Am. Chem. Soc. 2018, 140, 16580−16588

overpotential. In addition, PdCu-NP treated at 600 °C has a large size of 18.5 nm, but shows low SA (20 times lower than 500 °C-treated sample: 7.0 nm, close to 200 °C-treated sample: 4.7 nm). Obviously these HOR activity behaviors do not follow a trend based solely on size effect.

The PdCu/C-200 °C and PdCu/C-500 °C, as the less active and the most active HOR catalyst, were reanalyzed by using HAADF-STEM, respectively (Figure 6). The upper insets of

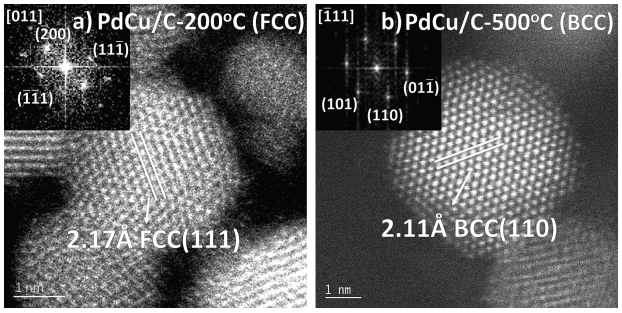

Figure 6. High-resolution HAADF STEM images of (a) PdCu/C-200 °C and (b) PdCu/C-500 °C. The insets of panels a and b are the corresponding FFT of FCC structure and BCC structure of PdCu along [011] and [$\bar{1}$ 11], respectively.

Figure 6 show the corresponding FFT patterns of the highlighted nanoparticle, indexed along the [011] and [$\bar{1}$ 11] zone axis, respectively. From Figure 6a, the average spacing of periodic lattice fringes was measured to be 2.17 Å, which can be assigned to the (111) facet of face-centered cubic (FCC) structured PdCu NPs. In contrast, a body-centered cubic (BCC) structure was detected from the PdCu/C-500 °C sample, where a clearly superperiodic BCC (110) facet with 2.11 Å lattice spacing can be distinguished. From PdCu/C-200 °C to PdCu/C-500 °C, the different crystalline structure suggests an FCC/BCC phase transformation during thermal annealing. Therefore, regular X-ray diffraction (XRD) characterization was used to study the crystalline structure of thermally annealed PdCu/C-*T* (*T* = 200 °C to 600 °C) catalysts. From XRD patterns of pristine PdCu/C-raw (Figure 7), a broad peak at 41.7° was observed. As the heat treatment temperature increased, this broad peak gradually shifted to a higher angle, and a shoulder peak evolved at 41.4°. In the end, the broad peak drastically splits into two sharp peaks at 41.4° and 42.9° under 600 °C thermal annealing, which can be well

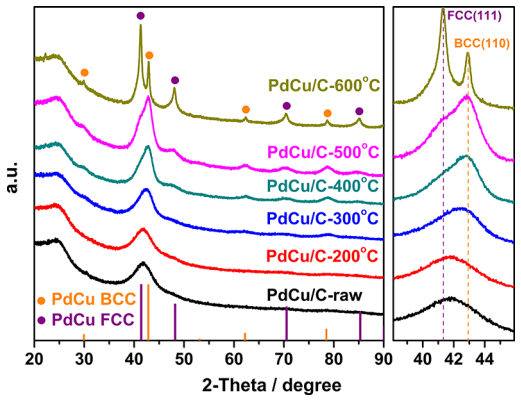

Figure 7. XRD patterns of PdCu/C-raw and PdCu/C-*T* (*T* = 200 °C to 600 °C).

assigned to FCC(111) (ICDD 00-048-1551) and CsCl-structure typed BCC(110) plane of PdCu (ICDD 04-015-2413). Moreover, the reflections of PdCu FCC(200), (220), and (311) facets were observed at 48.2°, 70.5°, and 85.3°, while the PdCu BCC (100), (200), and (211) facets were observed at 29.9°, 62.2°, and 78.5°, respectively. It turns out that the BCC structure of PdCu was formed via thermal annealing, which is indicated by the broad peak positive shift and the growth of corresponding BCC reflections in the high angle region. Despite distinct FCC (111) and BCC (110) peak separation observed on PdCu/C-600 °C, the integrated intensity of PdCu FCC (111) and BCC (110) peaks were overlapped among all investigated PdCu/C samples. To understand the mechanism of this FCC/BCC phase transformation during thermal annealing, the in situ high energy XRD (HE-XRD) (0.774902 Å wavelength) was carried out with the protocol of ramped annealing from 200 °C to 900 °C at 2 °C min^{-1} heating rate under UHP N_2 gas flow (Figure S6), and the 2D HE-XRD patterns were converted into a 3D color map of the intensity of FCC(111), BCC(110), and FCC(200) peaks (from 200 °C to 650 °C) shown in Figure 8.

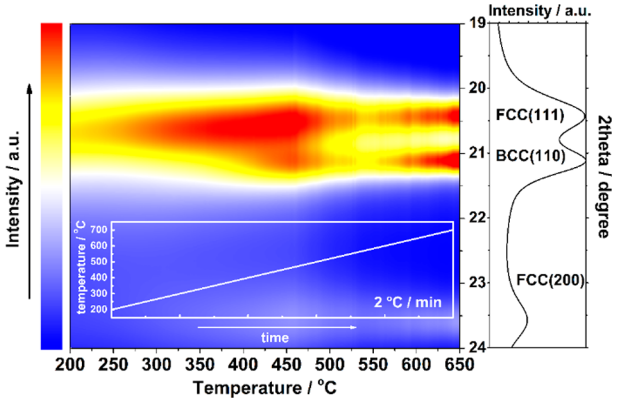

Figure 8. Color map of the intensity of peaks in the HE-XRD patterns (0.774902 Å wavelength) for PdCu/C-raw upon heating at the selected temperature range. The protocol of ramped annealing is from 200 °C to 900 °C at 2 °C min^{-1} heating rate under UHP N_2 gas flow.

A representative HE-XRD pattern collected at 600 °C shows three well-defined peaks, centered at 20.5°, 21.3°, and 23.8°, which can be assigned to FCC(111), BCC(110), and FCC(200) facets, respectively. From Figure 8 and Figure S6, it is obvious that the broad peak centered at 20.7° gradually splits to two peaks at ~270 °C, indicating the BCC structure formation. With further heating to 400 °C, the FCC (111) and BCC(110) diffraction peaks become distinct, followed by peak shrinking at ~450 °C. This peak shrinking implies that the particle size increased due to particle agglomeration, which is in good agreement with the TEM characterization results of PdCu/C-500 °C and PdCu/C-600 °C. As the temperature further increases to 900 °C, the FCC(111) diffraction peak becomes very sharp, while the BCC(110) peak becomes indistinguishable. It should be noted that the heating protocol of in situ HE-XRD (2 °C min^{-1}) without final temperature aging could cause an incomplete crystalline structure transformation of FCC/BCC. Therefore, FCC(111) and BCC(110) diffraction peak splitting can be observed at lower temperatures (<600 °C), which is fairly different from the broad peak positive shift observation at 4 h constant

DOI: 10.1021/jacs.8b08356
J. Am. Chem. Soc. 2018, 140, 16580−16588

temperature aged PdCu/C samples characterized by regular ex situ XRD.[37]

Aligned with the results from in situ HE-XRD and regular ex situ XRD, it is confirmed that partial FCC structured PdCu NPs started to transform to BCC-typed PdCu NPs at ~270 °C at a slow rate, and the FCC and BCC structured PdCu NPs could coexist over a broad temperature range up to 900 °C. Therefore, the percentage of BCC structured PdCu NPs in PdCu/C-T (T = 300 °C to 500 °C) should be much higher than that in PdCu/C-200 °C, which correlates well to HOR activity enhancement of PdCu/C-T (T = 300 °C to 500 °C). This phase transformation process of PdCu NPs was supported by the Pd−Cu bulk interface-based phase diagram which recognized that the CsCl-structure typed BCC-PdCu alloy was produced favorably in the intermediate temperature range of ca. 250 °C to 510 °C at an equal atomic percentage of Cu and Pd.[38,39]

To quantify the FCC/BCC phase ratio, the regular ex situ XRD patterns of PdCu/C-T (T = 200 °C to 600 °C) was analyzed by using the reference intensity ratio (RIR) quantitative analysis method[40,41] (for details of RIR quantitative analysis, see Supporting Information). As shown in Figure S7, the BCC is the primary phase toward PdCu NPs, and very similar FCC/BCC structure ratios of around 33.4%/66.6%, 34.8%/65.2%, and 32.8%/67.2% were obtained from PdCu/C-300 °C, -400 °C, and -500 °C samples, respectively. In contrast, the PdCu/C-200 and 600 °C show the reverse FCC/BCC structure ratios of 80.5%/19.5% and 71.3%/28.7%, and the FCC phase is dominant. Although, the peak overlap might result in a larger bias of relative FCC/BCC phase estimation especially in PdCu/C-200 °C, it is obvious that the thermal annealing (300 °C to 500 °C) significantly changes the PdCu NP structure from FCC to BCC phase, which agrees well with the enhanced HOR activity of PdCu/C-300 °C, -400 °C, and -500 °C samples (Figure S9a).

A PdCu NPs catalyst with a high BCC phase ratio has been synthesized to further study the importance of the BCC phase to HOR activity improvement. Through modifications of a previously reported wet-chemistry method, with different Pd and Cu precursor ratios, a BCC PdCu/C-400 °C* sample, with ~3.0 nm PdCu particles, was obtained after 400 °C thermal annealing (Figure S8a).[23] As shown in Figure S8b, the XRD diffraction peaks can be assigned to BCC (100), (110), (200), (210), and (211) facets. With the RIR quantitative analysis, the BCC phase concentration was determined to be >95.4%, indicating this sample was predominantly BCC crystalline. The HOR specific activity over all thermal-annealed PdCu/C catalysts is plotted as a function of BCC phase concentration in Figure S9a. The HOR activity of investigated PdCu/C catalysts is clearly proportional to their BCC phase concentration, and BCC PdCu/C-400 °C* with the highest BCC phase content of >95.4% exhibits a higher SA of 3.145 mA cm^{-2}_{Pd} at 100 mV overpotential. The SA of BCC PdCu/C-400 °C* (3.145 mA cm^{-2}_{Pd}) is very close to that of a commercial PtRu/C 20 wt % sample (3.286 mA cm^{-2}_{Pt}), which is the most active commercial HOR catalyst in alkaline media (Figure S9b).

By combining the experimental results of the relative FCC/BCC phase ratios and their corresponding HOR activities, it is highly possible to attribute the greatly enhanced HOR activity of PdCu/C-300 °C, -400 °C, and -500 °C and BCC PdCu-400 °C* to the generation of BCC crystalline phase. In comparison with FCC phase, the BCC structured PdCu NP contains a different geometrical structure, which may offer different H and OH adsorption strengths on the PdCu NP surface, so as to influence its HOR activity. Therefore, density functional theory (DFT) calculation was utilized to investigate the H and OH adsorption strengths on the specific crystal facet of BCC and FCC structured PdCu NPs and further elucidate the crystalline structure effect on its HOR activity enhancement in alkaline electrolyte.

DFT Computation of PdCu Catalysts for Alkaline HOR. Aiming to acquire theoretical insights into the different HOR activity for PdCu BCC and FCC surfaces, we explored both OH and H binding on PdCu structures that varied the combination of atom arrangements (FCC and BCC) and lattice constants to investigate the different impacts of atomic distances or atomic arrangements on H and OH binding. Three representative models of PdCu BCC(110) and FCC(111) surfaces were created (Figure S10) owing to their close-packed structure with relatively low surface energy. We refer to these as PdCu-B2(110), PdCu-$L1_0$(111), and PdCu-B13(111), respectively, as illustrated in a previous theoretical work.[42] Both the atomic arrangements and lattice constants and atomic arrangements could impact adsorption, such that both factors are necessary for optimal H and OH adsorption on Pd/PdCu-B2(110) compared to Pd/PdCu-$L1_0$ (111) and Pd/PdCu-B13(111) surfaces. In addition, the surface Pd enrichment observed in the experiments was also considered in these models by using a full Pd overlayer above the bimetallic subsurface (denoted as Pd/M, where M was the bimetallic surface) (for DFT model setup, see Supporting Information).

The 1/6 ML coverage H and 1/3 ML coverage OH adsorption potential values (denoted as U_{ad}(H) and U_{ad}(OH)) on these PdCu close-packed surfaces as well as those on Pt(111), Pd(111), and Cu(111) are shown in Figure 9. Note

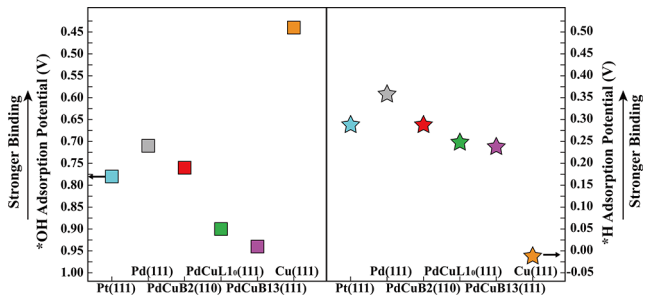

Figure 9. Equilibrium adsorption potentials (V_{RHE}) for *H (1/6 ML) and *OH (1/3 ML) on Pt, Pd, BCC-PdCu (B2 phase), and FCC-PdCu ($L1_0$ and B13 phases) terrace surfaces. The three PdCu surfaces shown here are covered by 1 ML Pd.

that the 1/3 ML OH adsorption model is only used to calculate OH adsorption potential and does not represent the real electrochemical interface status in HOR potential regions. We have investigated the coverage dependence of the H adsorption potential and found little variation with respect to coverage (Figure S11). H binding is the strongest on Pd(111) with the most positive adsorption potential (U_{ad}(H) = 0.36 V), and weakest on Cu(111) (U_{ad}(H) = −0.01 V). For the three PdCu alloy surfaces, U_{ad}(H) lie between that of pure Pd and Cu, namely, 0.29 V on Pd/PdCu-B2(110), 0.25 V on Pd/PdCu-$L1_0$(111), and 0.24 V on Pd/PdCu-B13(111), respectively. The U_{ad}(H) on these PdCu surfaces are much closer to that on Pt(111) (U_{ad}(H) = 0.29 V) than Pd(111) and

DOI: 10.1021/jacs.8b08356
J. Am. Chem. Soc. 2018, 140, 16580−16588

Cu(111) surfaces. The OH adsorption, contrarily, is strongest on Cu(111) (U_{ad}(OH) = 0.44 V) while much weaker on Pd(111) (U_{ad}(OH) = 0.71 V). However, on all of the three model PdCu surfaces, U_{ad}(OH) are higher than those on both Pd(111) and Cu(111), namely, 0.76 V on Pd/PdCu-B2(110), 0.90 V on Pd/PdCu-L1$_0$(111), and 0.94 V on Pd/PdCu-B13(111), respectively. The contradicting trends of U_{ad}(H) and U_{ad}(OH) on Pd/PdCu surfaces compared to pure Pd and Cu are consistent with those on Pd/Cu bimetallic surfaces (Figure S12), suggesting that the strain and ligand effects in the near surface PdCu alloy are maintained in Pd/PdCu systems.

Both H and OH adsorption potential values on Pd/PdCu-B2(110) are almost the same as those on Pt(111) (U_{ad}(H) = 0.29 V, U_{ad}(OH) = 0.78 V). It is well-known that Pt possesses the best alkaline HOR catalytic performance among all the pure metals; therefore, Pd/PdCu-B2(110) is anticipated to exhibit similar catalytic activity for alkaline HOR. The calculation results are in excellent accordance with experimental results that PdCu nanoparticles containing more BCC phase possess better HOR catalytic activity.

Comparing the adsorption potentials of H and OH on different Pd/PdCu surfaces with different crystalline structures of FCC and BCC, H adsorption is only a little weaker on the two Pd/PdCu-FCC(111) surfaces than on Pd/PdCu-B2(110) and Pt(111). The binding of H on Pt lies near the topmost of the activity volcano. If the adsorption potential of H is the single descriptor in effect, the HOR catalytic activity on Pd/PdCu-FCC(111) should be similar to those on Pd/PdCu-B2(110) and Pt(111), which contradicts the experiment. In sharp contrast, OH adsorption strength is weakened by ∼0.2 eV on Pd/PdCu-FCC(111) than on Pd/PdCu-B2(110) and Pt(111), suggesting that the lower oxophilicity of the FCC-PdCu(111) surfaces correlates with its relatively poor catalytic performance. Owing to different geometrical structures of BCC(110) and FCC(111) substrates and different extents of lattice compression of Pd overlayers, it shows a smaller weakened extent of both H and OH adsorption on Pd/PdCu-B2(110) than on Pd/PdCu-L1$_0$ (111) and Pd/PdCu-B13(111) surfaces as compared to the Pd(111) surface; therefore, BCC-phased PdCu could be more active than the FCC-phased PdCu. In summary, we argue that it is not sufficient to estimate the alkaline HOR catalytic activity of a given material by simply measuring the adsorption potential of H. Instead, different oxophilicity (OH binding energy) should also be taken into account.

To further explore the relation between HOR activity and H and OH adsorption strengths, we plot the experimentally obtained specific exchange current density ($i_{0,s}$) with DFT-calculated H and OH adsorption potentials, as illustrated in Figure 10 (for details of $i_{0,s}$ calculation, see Supporting Information and Table S4). The results suggest the pair of optimal H and OH adsorption potentials of ∼0.28 V and ∼0.75 V, respectively, at which the maximum HOR activity could be achieved. Compared with Pd/PdCu-BCC(110), the lower HOR performance on Pd/PdCu-FCC(111) is largely attributed to the weaker-than-optimal OH binding, i.e., the lower oxophilicity. Furthermore, due to the stronger OH binding on Co and Ni surfaces, the HOR exchange current densities are much lower on these metals in alkaline electrolytes, although the H adsorption potential on Co and Ni are similar to those on Pt. In summary, due to the closer H and OH adsorption potentials to the volcano top, PdCu-BCC phase exhibits HOR activity higher than that of all other tested materials.

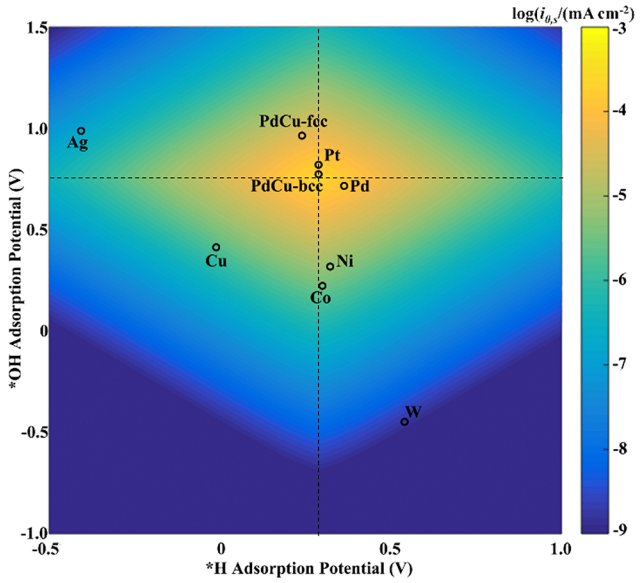

Figure 10. Experimentally measured exchange current density, log($i_{0,s}$), for hydrogen oxidation in base over different metals plotted with calculated H and OH adsorption potentials. The two dashed lines represent the optimal *H adsorption potential (∼0.28 V) and the optimal *OH adsorption potential (∼0.75 V), respectively.

CONCLUSIONS

In summary, we report that BCC-phase PdCu alloy nanoparticles were successfully synthesized by using a wet-chemical method, followed by a subsequent thermal annealing. The HOR activity of these PdCu catalysts strongly depends on the annealing temperature, and the PdCu/C-500 °C sample, featuring a dominant BCC crystalline structure, exhibits about 4 times and 2 times higher mass and specific activity than those of Pd/C and Pt/C in alkaline electrolyte. The crystalline structure transformation between FCC to BCC was observed during thermal annealing from 200 °C to 600 °C. At lower annealing temperature (<300 °C), the as-synthesized PdCu NPs are stabilized with FCC crystalline structure, while the higher annealing temperature (300 °C to 600 °C) results in a phase transformation from FCC to BCC. Consequently, the correlation of the crystalline structure of PdCu NPs with HOR activity was first created in this work, and it is demonstrated that the higher HOR activity of PdCu catalysts can be attributed to the BCC phase dominance. The DFT computations were used to further investigate HOR enhancement from the perspective of H and OH adsorption strength. As compared to the PdCu FCC model surface, the PdCu BCC model surface possesses very similar H binding and a much stronger OH binding, which are closer to those on the Pt model surface. Therefore, the BCC phase-dominated PdCu/C-500 °C catalysts exhibit higher HOR activity in alkaline electrolyte. By taking all results into consideration, the BCC-phased PdCu materials are promising as an alternative to Pt materials as the HOR catalyst for AEMFCs.

ASSOCIATED CONTENT

Supporting Information

The Supporting Information is available free of charge on the ACS Publications website at DOI: 10.1021/jacs.8b08356.

DOI: 10.1021/jacs.8b08356
J. Am. Chem. Soc. 2018, 140, 16580−16588

Experimental details, HOR mass and specific activity determination and exchange current density calculation with ECSA measurement details, durability test, supplemental voltammetry, TGA, TEM, and XPS and HE-XRD characterization results, RIR quantitative analysis, and DFT calculation details (PDF)

AUTHOR INFORMATION

Corresponding Author

*wzli@iastate.edu

ORCID

Yawei Li: 0000-0002-1271-4006

Wenzhen Li: 0000-0002-1020-5187

Author Contributions

‡Y.Q., L.X., and Y.L. contributed equally.

Notes

The authors declare no competing financial interest.

ACKNOWLEDGMENTS

This research was funded by the Iowa State University Start-Up Fund, Ames Laboratory Start-Up Fund, Iowa Energy Center. W. Li is grateful for his Bailey Research Career Development Award and Richard Seagrave Professorship. This research used resources of the Advanced Photon Source, a U.S. Department of Energy (DOE) Office of Science User Facility operated for the DOE Office of Science by Argonne National Laboratory under contract no. DE-AC02-06CH11357. We thank Dr. Dapeng Jing and Dr. Scott Schlorholtz (The Materials Analysis and Research Laboratory of the Iowa State University Office of Biotechnology) for XPS and TGA characterizations in this publication.

REFERENCES

(1) Sheng, W. C.; Bivens, A. P.; Myint, M.; Zhuang, Z. B.; Forest, R. V.; Fang, Q. R.; Chen, J. G.; Yan, Y. S. Non-precious metal electrocatalysts with high activity for hydrogen oxidation reaction in alkaline electrolytes. *Energy Environ. Sci.* **2014**, *7*, 1719−1724.

(2) Kibler, L. A. Hydrogen Electrocatalysis. *ChemPhysChem* **2006**, *7*, 985−991.

(3) Neyerlin, K. C.; Gu, W. B.; Jorne, J.; Gasteiger, H. A. Determination of Catalyst Unique Parameters for the Oxygen Reduction Reaction in a PEMFC. *J. Electrochem. Soc.* **2006**, *153*, A1955−A1963.

(4) Markovic, N. M.; Gasteiger, H. A.; Ross, P. N. Oxygen Reduction on Platinum Low-Index Single-Crystal Surfaces in Alkaline Solution: Rotating Ring Disk$_{Pt(hkl)}$ Studies. *J. Phys. Chem.* **1996**, *100*, 6715−6721.

(5) Piana, M.; Catanorchi, S.; Gasteiger, H. A. Kinetics of Non-Platinum Group Metal Catalysts for the Oxygen Reduction Reaction in Alkaline Medium. *ECS Trans.* **2008**, *16*, 2045−2055.

(6) Neyerlin, K. C.; Gu, W. B.; Jorne, J.; Gasteiger, H. A. Study of the Exchange Current Density for the Hydrogen Oxidation and Evolution Reactions. *J. Electrochem. Soc.* **2007**, *154*, B631−B635.

(7) Durst, J.; Simon, C.; Hasche, F.; Gasteiger, H. A. Hydrogen Oxidation and Evolution Reaction Kinetics on Carbon Supported Pt, Ir, Rh, and Pd Electrocatalysts in Acidic Media. *J. Electrochem. Soc.* **2015**, *162*, F190−F203.

(8) Durst, J.; Siebel, A.; Simon, C.; Hasche, F.; Herranz, J.; Gasteiger, H. A. New insights into the electrochemical hydrogen oxidation and evolution reaction mechanism. *Energy Environ. Sci.* **2014**, *7*, 2255−2260.

(9) Trasatti, S. Work function, electronegativity, and electrochemical behaviour of metals: III. Electrolytic hydrogen evolution in acid solutions. *J. Electroanal. Chem. Interfacial Electrochem.* **1972**, *39*, 163−184.

(10) Norskov, J. K.; Bligaard, T.; Logadottir, A.; Kitchin, J. R.; Chen, J. G.; Pandelov, S.; Stimming, U. Trends in the Exchange Current for Hydrogen Evolution. *J. Electrochem. Soc.* **2005**, *152*, J23−J26.

(11) Skulason, E.; Tripkovic, V.; Bjorketun, M. E.; Gudmundsdottir, S.; Karlberg, G.; Rossmeisl, J.; Bligaard, T.; Jonsson, H.; Norskov, J. K. Modeling the Electrochemical Hydrogen Oxidation and Evolution Reactions on the Basis of Density Functional Theory Calculations. *J. Phys. Chem. C* **2010**, *114*, 22374−22374.

(12) Sheng, W. C.; Myint, M.; Chen, J. G. G.; Yan, Y. S. Correlating the hydrogen evolution reaction activity in alkaline electrolytes with the hydrogen binding energy on monometallic surfaces. *Energy Environ. Sci.* **2013**, *6*, 1509−1512.

(13) Zheng, J.; Sheng, W. C.; Zhuang, Z. B.; Xu, B. J.; Yan, Y. S. Universal dependence of hydrogen oxidation and evolution reaction activity of platinum-group metals on pH and hydrogen binding energy. *Sci. Adv.* **2016**, *2*, e1501602.

(14) Sheng, W. C.; Zhuang, Z. B.; Gao, M. R.; Zheng, J.; Chen, J. G. G.; Yan, Y. S. Correlating hydrogen oxidation and evolution activity on platinum at different pH with measured hydrogen binding energy. *Nat. Commun.* **2015**, *6*, 5848.

(15) Strmcnik, D.; Uchimura, M.; Wang, C.; Subbaraman, R.; Danilovic, N.; van der Vliet, D.; Paulikas, A. P.; Stamenkovic, V. R.; Markovic, N. M. Improving the hydrogen oxidation reaction rate by promotion of hydroxyl adsorption. *Nat. Chem.* **2013**, *5*, 300−306.

(16) Li, J.; Ghoshal, S.; Bates, M. K.; Miller, T. E.; Davies, V.; Stavitski, E.; Attenkofer, K.; Mukerjee, S.; Ma, Z. F.; Jia, Q. Experimental Proof of the Bifunctional Mechanism for the Hydrogen Oxidation in Alkaline Media. *Angew. Chem., Int. Ed.* **2017**, *56*, 15594−15598.

(17) Wang, Y.; Wang, G. W.; Li, G. W.; Huang, B.; Pan, J.; Liu, Q.; Han, J. J.; Xiao, L.; Lu, J. T.; Zhuang, L. Pt-Ru catalyzed hydrogen oxidation in alkaline media: oxophilic effect or electronic effect? *Energy Environ. Sci.* **2015**, *8*, 177−181.

(18) McCrum, I. T.; Janik, M. J. pH and Alkali Cation Effects on the Pt Cyclic Voltammogram Explained Using Density Functional Theory. *J. Phys. Chem. C* **2016**, *120*, 457−471.

(19) Chen, X.; McCrum, I. T.; Schwarz, K. A.; Janik, M. J.; Koper, M. T. M. Co-adsorption of Cations as the Cause of the Apparent pH Dependence of Hydrogen Adsorption on a Stepped Platinum Single-Crystal Electrode. *Angew. Chem., Int. Ed.* **2017**, *56*, 15025−15029.

(20) Chung, H. T.; Choe, Y. K.; Martinez, U.; Dumont, J. H.; Mohanty, A.; Bae, C.; Matanovic, I.; Kim, Y. S. Effect of Organic Cations on Hydrogen Oxidation Reaction of Carbon Supported Platinum. *J. Electrochem. Soc.* **2016**, *163*, F1503−F1509.

(21) Scofield, M. E.; Zhou, Y. C.; Yue, S. Y.; Wang, L.; Su, D.; Tong, X.; Vukmirovic, M. B.; Adzic, R. R.; Wong, S. S. Role of Chemical Composition in the Enhanced Catalytic Activity of Pt-Based Alloyed Ultrathin Nanowires for the Hydrogen Oxidation Reaction under Alkaline Conditions. *ACS Catal.* **2016**, *6*, 3895−3908.

(22) Greeley, J.; Mavrikakis, M. Alloy catalysts designed from first principles. *Nat. Mater.* **2004**, *3*, 810−815.

(23) Jiang, K. Z.; Wang, P. T.; Guo, S. J.; Zhang, X.; Shen, X.; Lu, G.; Su, D.; Huang, X. Q. Ordered PdCu-Based Nanoparticles as Bifunctional Oxygen-Reduction and Ethanol-Oxidation Electrocatalysts. *Angew. Chem., Int. Ed.* **2016**, *55*, 9030−9035.

(24) Qiu, Y.; Xin, L.; Li, W. Z. Electrocatalytic Oxygen Evolution over Supported Small Amorphous Ni−Fe Nanoparticles in Alkaline Electrolyte. *Langmuir* **2014**, *30*, 7893−7901.

(25) Zheng, J.; Zhou, S. Y.; Gu, S.; Xu, B. J.; Yan, Y. S. Size-Dependent Hydrogen Oxidation and Evolution Activities on Supported Palladium Nanoparticles in Acid and Base. *J. Electrochem. Soc.* **2016**, *163*, F499−F506.

(26) Sheng, W. C.; Gasteiger, H. A.; Shao-Horn, Y. Hydrogen Oxidation and Evolution Reaction Kinetics on Platinum: Acid vs Alkaline Electrolytes. *J. Electrochem. Soc.* **2010**, *157*, B1529−B1536.

DOI: 10.1021/jacs.8b08356
J. Am. Chem. Soc. 2018, 140, 16580−16588

(27) Fang, L. L.; Tao, Q. A.; Li, M. F.; Liao, L. W.; Chen, D.; Chen, Y. X. Determination of the Real Surface Area of Palladium Electrode. *Chin. J. Chem. Phys.* **2010**, *23*, 543−548.
(28) Shao, M. H.; Odell, J. H.; Choi, S. I.; Xia, Y. N. Electrochemical surface area measurements of platinum- and palladium-based nanoparticles. *Electrochem. Commun.* **2013**, *31*, 46−48.
(29) Lorimer, J. P.; Mason, T. J.; Plattes, M.; Walton, D. J. Passivation phenomena during sonovoltammetric studies on copper in strongly alkaline solutions. *J. Electroanal. Chem.* **2004**, *568*, 379−390.
(30) Hara, M.; Linke, U.; Wandlowski, Th. Preparation and electrochemical characterization of palladium single crystal electrodes in 0.1 M H_2SO_4 and $HClO_4$: Part I. Low-index phases. *Electrochim. Acta* **2007**, *52*, 5733−5748.
(31) Lu, L. F.; Lou, B. H.; Zou, S. H.; Kobayashi, H.; Liu, J. J.; Xiao, L. P.; Fan, J. Robust Removal of Ligands from Noble Metal Nanoparticles by Electrochemical Strategies. *ACS Catal.* **2018**, *8*, 8484−8492.
(32) Zhang, Z. Y.; Xin, L.; Sun, K.; Li, W. Z. Pd-Ni electrocatalysts for efficient ethanol oxidation reaction in alkaline electrolyte. *Int. J. Hydrogen Energy* **2011**, *36*, 12686−12697.
(33) Yang, N. L.; Zhang, Z. C.; Chen, B.; Huang, Y.; Chen, J. Z.; Lai, Z. C.; Chen, Y.; Sindoro, M.; Wang, A. L.; Cheng, H. F.; Fan, Z. X.; Liu, X. Z.; Li, B.; Zong, Y.; Gu, L.; Zhang, H. Synthesis of Ultrathin PdCu Alloy Nanosheets Used as a Highly Efficient Electrocatalyst for Formic Acid Oxidation. *Adv. Mater.* **2017**, *29*, 1700769.
(34) Shao, M. H.; Peles, A.; Shoemaker, K. Electrocatalysis on Platinum Nanoparticles: Particle Size Effect on Oxygen Reduction Reaction Activity. *Nano Lett.* **2011**, *11*, 3714−3719.
(35) Nesselberger, M.; Ashton, S.; Meier, J. C.; Katsounaros, I.; Mayrhofer, K. J.; Arenz, M. The Particle Size Effect on the Oxygen Reduction Reaction Activity of Pt Catalysts: Influence of Electrolyte and Relation to Single Crystal Models. *J. Am. Chem. Soc.* **2011**, *133*, 17428−17433.
(36) Tan, T. L.; Wang, L.; Zhang, J.; Johnson, D. D.; Bai, K. W. Platinum Nanoparticle During Electrochemical Hydrogen Evolution: Adsorbate Distribution, Active Reaction Species, and Size Effect. *ACS Catal.* **2015**, *5*, 2376−2383.
(37) Thönnessen, L., Influence of heat treatment parameters on phase transformations in the near-beta titanium alloy Ti-1Al-8V-5Fe. Ph.D. Thesis. School of Mechanical, Materials, Mechatronic and Biomedical Engineering, University of Wollongong, 2017.
(38) Subramanian, P. R.; Laughlin, D. E. Cu-Pd (Copper-Palladium). *J. Phase Equilib.* **1991**, *12*, 231−243.
(39) Rudashevsky, N. S.; McDonald, A. M.; Cabri, L. J.; Nielsen, T. F. D.; Stanley, C. J.; Kretzer, Y. L.; Rudashevsky, V. N. Skaergaardite, PdCu, a new platinum-group intermetallic mineral from the Skaergaard intrusion, Greenland. *Mineral. Mag.* **2004**, *68*, 615−632.
(40) Hillier, S. Accurate quantitative analysis of clay and other minerals in sandstones by XRD: comparison of a Rietveld and a reference intensity ratio (RIR) method and the importance of sample preparation. *Clay Miner.* **2000**, *35*, 291−302.
(41) Omotoso, O.; Mccarty, D. K.; Hillier, S.; Kleeberg, R. Some successful approaches to quantitative mineral analysis as revealed by the 3rd reynolds cup contest. *Clays Clay Miner.* **2006**, *54*, 748−760.
(42) Sha, Y.; Yu, T. H.; Merinov, B. V.; Goddard, W. A. DFT Prediction of Oxygen Reduction Reaction on Palladium-Copper Alloy Surfaces. *ACS Catal.* **2014**, *4*, 1189−1197.

DOI: 10.1021/jacs.8b08356
J. Am. Chem. Soc. 2018, 140, 16580−16588